The Plant Journal (2007) **50**, 1020–1034 doi: 10.1111/j.1365-313X.2007.03106.x

The Arabidopsis cohesin protein SYN3 localizes to the nucleolus and is essential for gametogenesis

Ling Jiang, Ming Xia†, Lara I. Strittmatter and Christopher A. Makaroff*
Department of Chemistry and Biochemistry, Miami University, Oxford, OH 45056, USA

Received 01 December 2006; revised 14 February 2007; accepted 21 February 2007.
*For correspondence (fax + 1 513 529 5715; email makaroca@muohio.edu).
†Present address: Division of Infectious Diseases, Cincinnati Children's Hospital Medical Center, 3333 Burnet Avenue, Cincinnati, OH 45229, USA.

Summary

α-kleisins are core components of meiotic and mitotic cohesin complexes. Arabidopsis contains genes for four α-kleisin proteins encoded by *SYN* genes. *SYN1*, a *REC8* ortholog, is essential for meiosis, while *SYN2* and *SYN4* appear to be *SCC1* orthologs and function in mitosis. Our analysis of At*SYN3* shows that it localizes primarily in the nucleolus of both meiotic and mitotic cells. Furthermore, analysis of plants containing an At*SYN3* T-DNA knockout mutation demonstrated that it is essential for megagametogenesis and plays an important role in pollen. These results suggest that SYN3 may not function as part of a typical cohesin complex; rather it may have evolved a specialized role in controlling rDNA structure, transcription or rRNA processing.

Keywords: cohesin, mitosis, gametogenesis, meiosis, nucleolus, kleisin.

Introduction

During nuclear division, the replicated copies of each chromosome are held together by a multi-subunit complex of proteins, termed the cohesin complex, until their segregation at anaphase. The proper formation and subsequent release of sister chromatid cohesion is essential for chromosome condensation, their bipolar attachment to the spindle, and ultimately their correct segregation at anaphase (Nasmyth, 2001; Uhlmann, 2004). The cohesin complex consists of a heterodimer of the 'structural maintenance of chromosome' (SMC) proteins SMC1 and SMC3, and two non-SMC proteins, SCC3 and SCC1/MCD1/RAD21 (hereafter referred to as SCC1) (Losada and Hirano, 2005; Nasmyth and Haering, 2005).

SMC1 and SMC3 form the core of the cohesin complex. They interact at their hinge domains, forming a ring-shaped structure with a central hole large enough for two nucleosomal DNA fibers (Haering *et al.*, 2002). SCC1 appears to be the regulatory subunit of the complex. The N-terminus of SCC1 binds the head domain of SMC3, while the C-terminus of SCC1 binds the head domain of SMC1 (Haering *et al.*, 2002, 2004), thereby closing the cohesin ring complex. SCC1 is cleaved by separase, a cysteine proteinase, releasing cohesion at the metaphase to anaphase transition (Uhlmann *et al.*, 2000). In addition, SCC1, along with SCC3, contain phosphorylation sites that are involved in the separase-independent removal of cohesin during mitotic prophase in animal cells (Losada *et al.*, 2002; Sumara *et al.*, 2002; Hauf *et al.*, 2005). Two different mitotic cohesin complexes containing different forms of SCC3 have been isolated from human cells (Losada *et al.*, 2000; Sumara *et al.*, 2000), and, in yeast, SCC3 was found to bind the C-terminal region of SCC1 (Haering *et al.*, 2002).

SCC1 belongs to a superfamily of proteins termed kleisins (Schleiffer *et al.*, 2003). The α-kleisins include SCC1 and its meiotic counterpart REC8, which are important for cohesion. The β- and γ-kleisins bind SMC2 and SMC4 and are found in condensin complexes (Ono *et al.*, 2003), while δ-kleisins bind SMC5 and SMC6 and are involved in double-strand DNA break repair (Nasmyth and Haering, 2005). Budding and fission yeast contain two α-kleisins, SCC1 and REC8, that are essential for mitosis and meiosis, respectively. In contrast, *Caenorhabditis elegans* contains four α-kleisin genes. REC8 was shown to participate in meiosis, while SCC1/COH-2 appears to be the mitotic cohesin (Pasierbek *et al.*, 2001). COH-1 has been shown to play a role in development that is unrelated to mitosis, while a mutation in

COH-3 failed to produce detectable abnormalities (Mito *et al.*, 2003).

Plants also contain four α-kleisin genes. Arabidopsis SYN1 (DIF1) and maize AFD1 have been identified as plant REC8 orthologs (Peirson *et al.*, 1997; Bai *et al.*, 1999; Bhatt *et al.*, 1999; Golubovskaya *et al.*, 2006). SYN1 labels meiotic chromosome axes from leptotene to metaphase I and is essential for sister chromatid cohesion and homologous chromosome pairing during meiosis (Cai *et al.*, 2003). Three other Arabidopsis α-kleisins genes, *SYN2*, *SYN3* and *SYN4*, have been identified, and are expressed throughout the plant, with high transcript levels observed in meristematic regions (Dong *et al.*, 2001). A recent study suggested that SYN2/AtRAD21.1 and SYN4/AtRAD21.3 may represent mitotic cohesins, with SYN2/AtRAD21.1 playing an additional role in DNA repair after ionizing radiation (da Costa-Nunes *et al.*, 2006). The results presented here indicate that AtSYN3/AtRAD21.2 plays a critical role in the nucleolus.

In addition to their essential role in chromosome segregation during mitosis and meiosis, cohesin complexes have been implicated in several other processes, including DNA double-strand break (DSB) repair and prevention of unequal sister chromatid recombination. Fission and budding yeast cohesin mutants, as well as *Xenopus* cells depleted for cohesin proteins, are hypersensitive to DNA damage (Birkenbihl and Subramani, 1992; Losada *et al.*, 1998; Klein *et al.*, 1999; Sonoda *et al.*, 2001). Further support for the role of cohesins in DNA DSB repair comes from observations that RAD21 and SMC1 are specifically recruited to sites of DNA damage after induction of DSBs in yeast and human cells, respectively (Kim *et al.*, 2002; Strom *et al.*, 2004; Unal *et al.*, 2004). It is currently thought that RAD21 DNA DSB repair activity is due to its cohesin function, ensuring correct chromosome topology and the physical proximity of sister chromatids in the S and G_2 phases, rather than a catalytic role in DNA repair. Furthermore, in yeast, SCC1 binding to the rDNA array has been shown to enhance genomic stability by preventing unequal sister chromatid exchange and/or regulating transcription of rDNA genes (Kobayashi *et al.*, 2004; Kobayashi and Ganley, 2005).

Although the specific role of α-kleisins in other cellular functions is less clear, it appears that they may also play important roles in growth and development that are not directly related to cell division. For example, in *C. elegans*, COH-1 is present on chromosomes in all somatic cells from approximately the 100-cell embryo stage through adulthood, and its depletion did not result in cell-cycle-related abnormalities (Mito *et al.*, 2003). While *coh-1* RNAi animals looked morphologically normal, they exhibited severe defects in locomotion, suggesting that COH-1 has important functions unrelated to nuclear division.

In this report, we present a detailed analysis of AtSYN3. Localization studies using anti-SYN3 antibody, as well as transgenic plants expressing SYN3–YFP and SYN3-Myc-tagged proteins, show that SYN3 localizes primarily in the nucleolus of both somatic cells and meiocytes. Analysis of a *SYN3* T-DNA insertion mutant demonstrated that it is an essential gene for both male and female gametophyte development. Reciprocal crosses between *Atsyn3*$^{+/-}$ and wild-type plants demonstrated that the *Atsyn3* mutation is transmitted at a reduced frequency through the pollen, and not at all through the egg. Alterations in megagametogenesis were detected in *Atsyn3*$^{+/-}$ plants beginning at female gametophyte stage 6 (FG6). Although pollen development appears relatively normal, subtle alterations in pollen morphology and reduced levels of pollen germination were consistently observed with *Atsyn3*$^{+/-}$ plants. These results suggest that SYN3 may have evolved a specialized role in the nucleolus that could involve enhancing genomic stability by preventing unequal sister chromatid exchange at the rDNA loci and/or regulating transcription of the rDNA genes.

Results

SYN3 localization

Localization studies were performed on SYN3 in order to gain insight into its cellular function. A 271 amino acid segment (amino acids 239–510) of SYN3 corresponding to the divergent middle portion of the protein was overexpressed as a 6xHis-tagged protein, purified and used to raise polyclonal antibody in rabbits.

When the antibody was used in immunolocalization studies on somatic cells and microsporocytes in anther squashes, as well as on Arabidopsis suspension culture cells, it labeled the nucleus throughout most of the cell cycle (Figure 1). While weak labeling was typically detected throughout the nucleoplasm, the strongest anti-SYN3 labeling was found in the nucleolus. In Arabidopsis suspension culture cells, strong SYN3 labeling was observed in the nucleolus from G_1 through early mitotic prophase (Figure 1a,b). The SYN3 signal became significantly weaker during nucleolar breakdown (Figure 1c) and was undetectable during metaphase and anaphase (Figure 1d,e). SYN3 signal was detected again in late telophase as the nucleoli began to reform (data not shown).

Non-specific labeling of the nucleolus with antibodies is sometimes observed in plant cells. Therefore, in order to test whether the nucleolar labeling pattern we observed for SYN3 was specific, we generated transgenic plants that express SYN3 tagged at its C-terminus with either the yellow fluorescent protein (YFP) or the Myc tag. Immunolocalization studies on somatic cells from SYN3-Myc transgenic plants using anti-Myc antibody (Figure 1f–j), as well as direct observation of anther squashes of SYN3–YFP transgenic plants with fluorescence microscopy (data not shown), yielded images similar to those observed with the SYN3

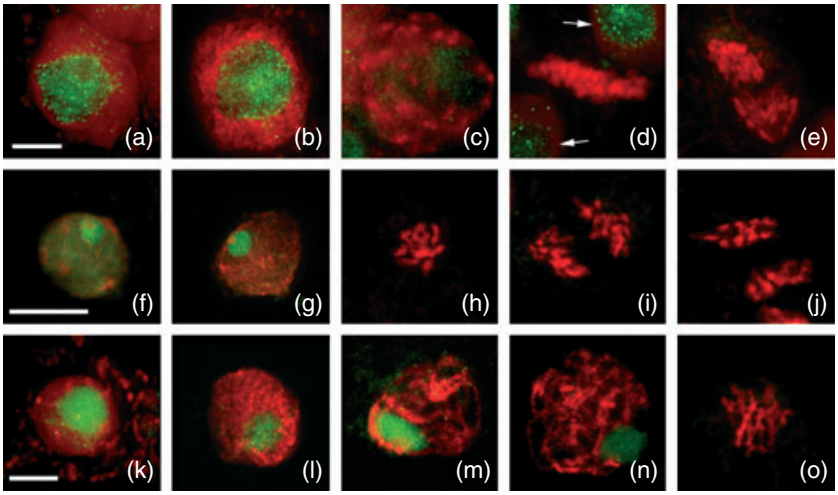

Figure 1. Localization of AtSYN3 in Arabidopsis somatic cells and microsporocytes.
The DAPI signal is red, and the antibody signal is green. AtSYN3 in suspension cells detected with anti-SYN3 antibody (a–e). AtSYN3 in anther somatic cells (f–j) and meiocytes (k–o) from transgenic plants expressing SYN3-Myc detected with anti-Myc antibody.
(a) Mitotic interphase. (b) Early prophase. (c) Late prophase. (d) Metaphase. Two interphase cells (arrows) are also shown. (e) Anaphase. (f) Mitotic interphase. (g) Prophase. (h) Metaphase. (i) Anaphase. (j) Telophase. (k) Meiotic interphase. (l) Lepotene. (m) Zygotene. (n) Pachytene. (o) Diplotene. Scale bars = 10 μm.

antibody. Strong SYN3 labeling of the nucleolus was observed from G_1 to prophase. However, localization experiments using transgenic SYN3-Myc plants typically detected stronger labeling in the nucleoplasm at interphase than did the anti-SYN3 antibody, suggesting that the C-terminal tag may have an effect on the protein's structure/function (Figure 1f).

Localization studies on anther squashes indicated that SYN3 also localizes in the nucleolus of microsporocytes. Strong SYN3 signal was found inside the nucleolus from meiotic interphase to late diplotene when the nucleoli broke down (Figure 1k–o). Weak diffuse labeling was also detected in the nucleoplasm, with the weakest signals observed from metaphase to telophase II. Therefore, in contrast to other plant cohesin proteins, which are found throughout the nucleus (Cai *et al.*, 2003; Chelysheva *et al.*, 2005; Lam *et al.*, 2005), SYN3 appears to localize predominately in the nucleolus.

Mutations in AtSYN3 *cause gametophyte lethality*

Two individual insertion lines, *Atsyn3-1* (SALK119629) and *Atsyn3-2* (09510A), with insertions in the 5′ UTR and the 5′ end of exon 6 of *AtSYN3*, respectively (Figure 2a), were identified and characterized to investigate the function of *AtSYN3*. PCR analysis of plants containing the *Atsyn3-1* insertion indicated that approximately 25% of the progeny from *Atsyn3-1*$^{+/-}$ plants were homozygous for the T-DNA insert. Southern blot analysis using a probe that spans the *AtSYN3-1* T-DNA insertion site confirmed that plants classified as homozygous for the *Atsyn3-1* insert did in fact contain two copies of the T-DNA insert (data not shown).

RT-PCR was performed on total RNA isolated from *Atsyn3-1*$^{-/-}$ plants, and showed that *AtSYN3* transcripts are present at approximately the same level in wild-type and *Atsyn3-1*$^{-/-}$ plants (Figure 2b). Taken together, these results indicate that the *Atsyn3-1* T-DNA insert has little or no effect on *AtSYN3* expression. Consistent with this finding was our observation that *Atsyn3-1*$^{-/-}$ plants appeared normal, and showed no significant alterations in growth, development or fertility. It is however possible that a subtle alteration may have gone undetected. The *Atsyn3-1* insertion line was therefore not characterized further.

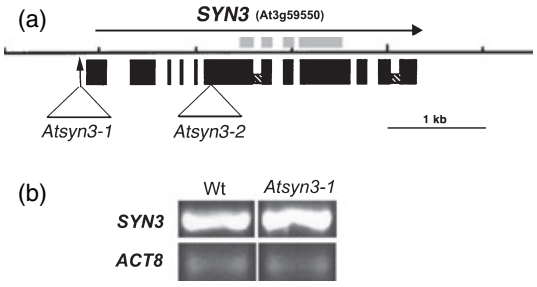

Figure 2. *AtSYN3* locus and T-DNA insertion lines.
(a) *AtSYN3* gene map. The position of intron and exon sequences, and the *Atsyn3-1* (SALK119629) and *Atsyn3-2* (09510A) T-DNA insertions are shown. A 271 amino acid region (gray blocks) that was used to produce the antibody is shown above the gene map.
(b) *AtSYN3* transcripts in buds of wild-type and *Atsyn3-1* homozygous plants. *ACT8* transcripts were used as the control.

In contrast, no homozygous *Atsyn3-2* plants were identified in over 300 plants examined. When seeds from *Atsyn3-2*$^{+/-}$ plants were collected, re-sown, and subjected to PCR analysis, we found that 74% of the progeny (242/327) were wild-type, whereas 26% were heterozygous for the *Atsyn3-2* insertion. These results indicated that *AtSYN3* is an essential gene, and suggest that the *Atsyn3-2* mutation causes gametophyte lethality. To investigate this possibility further, we backcrossed *Atsyn3-2*$^{+/-}$ plants with wild-type plants as both the male and female parent. When *Atsyn3-2*$^{+/-}$ plants were used as the female parent, we obtained 50 wild-type plants and no *Atsyn3-2*$^{+/-}$ plants. Crosses using *Atsyn3-2*$^{+/-}$ plants as the male parent produced 126 (73%) wild-type and 46 *Atsyn3-2*$^{+/-}$ plants. Similar ratios of wild-type and *Atsyn3-2*$^{+/-}$ plants were obtained over several backcross generations, consistent with a tight linkage between the observed lethality and the *Atsyn3-2* mutation. These results demonstrate that *AtSYN3* is essential for the development of functional female gametophytes, and indicate that the mutation is transmitted through pollen at a reduced frequency.

No obvious morphological changes, including seed germination, vegetative growth, inflorescence and flower development, were identified in *Atsyn3-2*$^{+/-}$ plants, with the exception that their siliques were shorter and contained reduced numbers of seed (18 ± 3 per silique versus 45 ± 6 per silique in wild-type plants, $n = 50$), as expected for a mutation that affects the female gametophyte.

Analysis of anthers from *Atsyn3-2*$^{+/-}$ plants failed to identify dramatic alterations in anther morphology or pollen development. When observed by scanning electron microscopy, some pollen grains from *Atsyn3-2*$^{+/-}$ plants showed a subtle decrease in length along the aperture, which altered their shape, while other pollen grains were shrunken. Abnormal pollen accounted for approximately 30% of all pollen grains from *Atsyn3-2*$^{+/-}$ plants (Figure 3a). Such alterations were not observed in wild-type plants. A light microscopy analysis of semi-thin sections through anthers at stages 11 and late 12 (Sanders *et al.*, 1999) failed to identify specific developmental abnormalities that could result in the altered sizes and shapes observed (Figure 3b). DAPI staining of mature pollen from *Atsyn3-2*$^{+/-}$ plants demonstrated that the vast majority, if not all, of the pollen contained two sperm nuclei and a vegetative nucleus, indicating that mitosis is not disrupted by the mutation (Figure 3c). Furthermore, no significant differences in pollen viability were observed between wild-type and *Atsyn3-2*$^{+/-}$ plants using TTC (2,3,5-triphenyl tetrazolium chloride) (Figure 3d). Pollen from *Atsyn3-2*$^{+/-}$ plants did however exhibit reduced germination frequencies (approximately 60% of wild-type levels, 36 ± 8% versus 60 ± 7%) when analyzed using an *in vitro* germination assay (Figure 3d). Therefore, although pollen containing the *Atsyn3-2* T-DNA insert appears to develop

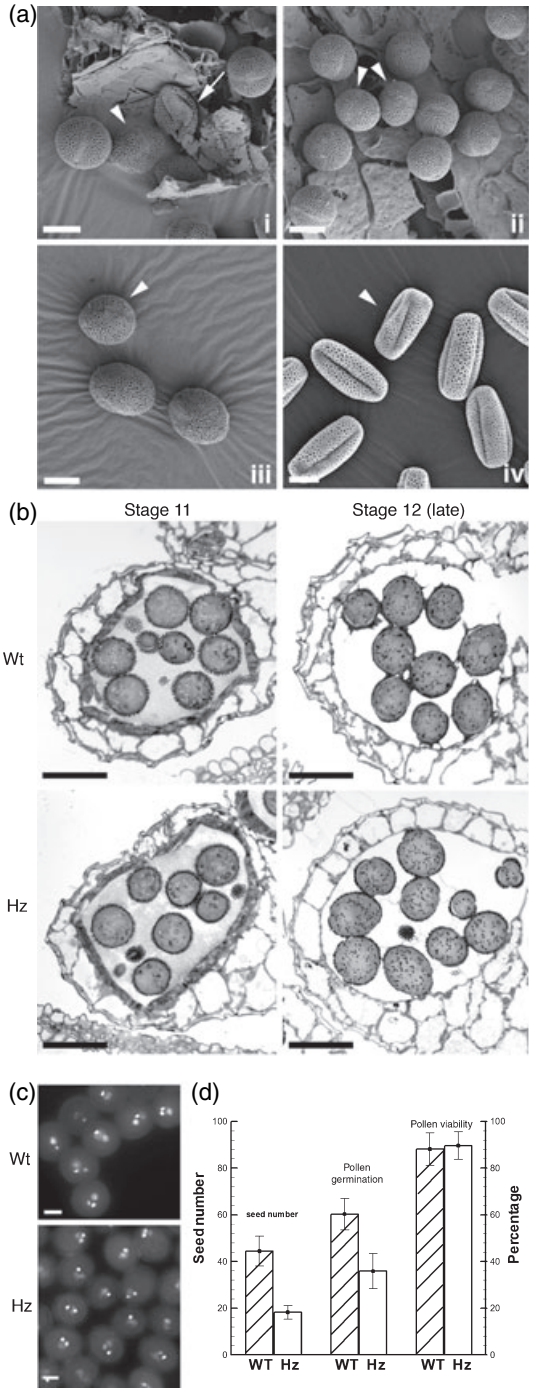

Figure 3. *Atsyn3-2*$^{+/-}$ pollen.
(a) SEM micrographs of a mixed population of *Atsyn3-2*$^{+/-}$ pollen. Pollen grains in images (i) to (iii) were fixed and critically point dried. Pollen grains in (iv) were air-dried. Approximately 30% of the pollen grains appear as either shrunken (arrow) or compact (shorter along the aperture, arrowhead).
(b) Bright-field micrographs of anther locule cross-sections. Wild-type and *Atsyn3-2*$^{+/-}$ locules at stages 11 and late 12 are shown.
(c) DAPI-stained wild-type and *Atsyn3-2*$^{+/-}$ mature pollen grains. Three nuclei (one vegetative and two sperm) can be seen in most pollen grains.
(d) Histogram comparing seed number, pollen germination and pollen viability in wild-type and *Atsyn3-2*$^{+/-}$ plants.
Scale bars = 10 μm in (a) and (c) and 25 μm in (b).

normally and is viable, a fraction of the pollen is not able to germinate.

AtSYN3 *is essential for the development of functional megagametophytes*

The effect of the *Atsyn3-2* mutation on megagametogenesis and embryo development was characterized by comparing pistil and embryo development in wild-type and At*syn3-2*$^{+/-}$ plants using confocal laser scanning microscopy (CLSM). Female gametophyte development was defined according to the method described by Christensen *et al.* (1998). As a reference for our results for *Atsyn3-2*$^{+/-}$ plants, wild-type development is shown in Figure 4. Prior to meiosis, a megaspore mother cell with a relatively large nucleus is observed in the ovules (Figure 4a). The megasporocyte undergoes meiosis to form a tetrad of haploid megaspores, and the three megaspores at the micropylar pole subsequently degenerate (Figure 4b). The remaining megaspore enlarges and adopts a teardrop shape with its nucleus in the center; this stage is defined as the uni-nucleate stage, FG1. The functional megaspore then undergoes mitosis to form a two-nucleate female gametophyte at FG2. FG3 is characterized by a gametophyte that contains a prominent central vacuole that separates the two nuclei at the chalazal and micropylar poles (Figure 4c). During stage FG4, the two nuclei undergo a second, simultaneous round of mitosis to produce a four-nucleate gametophyte (Figure 4d). A third round of mitosis during FG5 produces an eight-nucleate coenocytic embryo sac with four nuclei at each pole. A single nucleus at the chalazal pole then migrates toward the micropylar pole, giving rise to one of the two polar nuclei. Cellularization leads to the formation of seven cells: an egg cell and two synergids at the micropylar pole, three antipodal cells at the chalazal pole, and a central cell harboring the two polar nuclei (Figure 4e). By the beginning of FG6, the two polar nuclei have fused to form a diploid central cell nucleus, followed by degeneration of the three antipodal cells (Figure 4f). The complete disappearance of the antipodal cells marks the onset of FG7. At this stage, the female gametophyte consists of the central cell, the egg and two synergids (Figure 4g). FG8 is marked by degeneration of one of the synergid cells, which occurs after the pollen tube enters the female gametophyte by penetrating that synergid cell.

Double fertilization marks the end of female gametophyte development and the beginning of embryogenesis. One sperm nucleus fuses with the egg nucleus to form the zygote, while the other sperm nucleus fuses with the diploid central cell to form the triploid endosperm primary nucleus (Figure 4h). The fertilized central cell then divides into two endosperm nuclei, which migrate to the chalazal and micropylar poles, respectively (Figure 4i). Multiple rounds of nuclear division occur in the endosperm until cellularization finally occurs at the heart stage of embryo development. Subsequent to the onset of nuclear division in the endosperm, the zygote divides to form an embryo composed of the embryo proper and the suspensor. In Arabidopsis, the suspensor is a filamentous structure composed of an enlarged basal cell and a file of 6–8 additional cells. The embryo proper undergoes successive rounds of division to form the two-cell, quadrant, octant (Figure 4j), dermatogen, early globular, globular, heart, torpedo and mature embryos, respectively.

Female gametogenesis was analyzed in *Atsyn3-2*$^{+/-}$ plants. A total of 45 pistils at various stages of development from four different *Atsyn3-2*$^{+/-}$ plants were analyzed by CLSM. No abnormalities were found from archesporial cell development to approximately stage FG5 (Table 1). However, by the time wild-type gametophytes had reached FG6, a relatively large number of defects were observed. At this stage, 24% of the female gametophytes examined in *Atsyn3-2*$^{+/-}$ plants exhibited abnormalities (Table 1). Defects observed included totally degenerated embryo sacs (Figure 5a), and those that contained one nucleus (Figure 5b), two nuclei (Figure 5c), three nuclei (Figure 5d) or four nuclei (Figure 5e–h). In all abnormal embryo sacs, the position of the nuclei in the embryo sac was not normal. For example, abnormal female gametophytes with four nuclei did not resemble typical FG4 embryo sacs, which contain two nuclei at each pole. Rather the nuclei appeared to be randomly dispersed in the embryo sac. Figure 5(f–h) shows three optical sections of a four-nucleate embryo sac with one nucleus near the center of the embryo sac and the remaining three nuclei near the micropylar pole. Prior to fertilization, embryo sacs with four irregularly placed nuclei were the most common alteration observed, occurring approximately 37% of the time (Table 1). Some siliques contained a mixture of two or three types of abnormal embryo sacs, but typically multiple types of alterations were not found in one silique. By FG8, approximately 25% of the embryo sacs exhibited alterations, which ranged from totally degenerated embryo sacs to those with four irregularly spaced nuclei.

In carpels of *Atsyn3-2*$^{+/-}$ plants slightly later in development, we observed many of the same abnormalities plus several new phenotypes. After fertilization, degenerated embryo sacs (Figure 5i) were the most common phenotype observed (Table 1). Embryo sacs with three or four nuclei were also observed. In addition, abnormal seeds containing a degenerated zygote and a fertilized central cell were observed (Figure 5j). In these embryo sacs, the fertilized central cell sometimes appeared to undergo nuclear division to produce two endosperm nuclei before degeneration (Figure 5k). Finally, a very small number of seeds (four of 748 observed) were found to contain a four-cell embryo with cellularized endosperm (Figure 5l). By the time wild-type embryos were at the heart stage, the percentage of degenerated/abnormal seeds in siliques had increased to 57% (Table 1). Therefore, while some gametophytes appear to

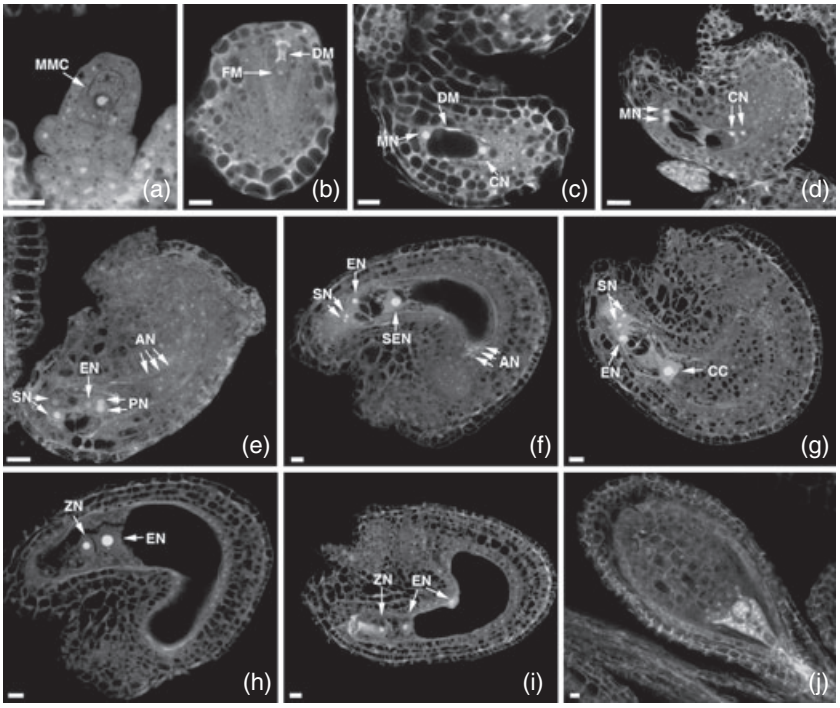

Figure 4. Female gametophyte and seed development in wild-type siliques revealed by CLSM.
Unless otherwise noted, the images consist of a single 1.5 μm optical section.
(a) Female gametophyte at stage FG0. The megaspore mother cell (MMC) is shown.
(b) Female gametophyte at stage FG1. A uni-nucleate functional megaspore (FM) and degenerating megaspores (DM) are shown.
(c) Female gametophyte at stage FG3. One nucleus is located at the chalazal pole (CN) and the other is at the micropylar pole (MN) of the embryo sac. Degenerating megaspores (DM) are visualized by their strong autoflorescence. A projection of two 1.5 μm optical sections is shown.
(d) Female gametophyte at stage FG4. Two micropylar nuclei (MN) and two chalazal nuclei (CN) are shown. A projection of three 1.5 μm optical sections is shown.
(e) Female gametophyte at late stage FG5. Three antipodal nuclei (AN), synergid cell nuclei (SN), the two polar nuclei (PN) and the egg cell nucleus (EN) are shown. A projection of four 1.5 μm optical sections is shown.
(f) Female gametophyte at stage FG6. The polar nuclei have fused, yielding the secondary endosperm nucleus (SEN). A projection of seven 1.5 μm optical sections is shown.
(g) Female gametophyte at stage FG7. A projection of four 1.5 μm optical sections is shown.
(h) Fertilized embryo sac that contains a zygote (ZN) and a fertilized central cell (endosperm nucleus, EN). A projection of two 2 μm optical sections is shown.
(i) Developing seed that contains an elongated zygote (nucleus, ZN) and two divided endosperm nuclei (EN). A projection of three 3 μm optical sections is shown.
(j) Octant embryo. A projection of five 3 μm optical sections is shown.
Scale bar = 10 μm.

develop to FG8 and are fertilized, these results indicate that all *Atsyn3-2*$^{-}$ megagametophytes are in fact not functional.

Our observation that approximately 25% of the embryo sacs in *Atsyn3-2*$^{+/-}$ plants arrest prior to fertilization, but that the remaining 25%, which should carry the *Atsyn3-2* T-DNA insert, appeared to be fertilized before degenerating, led us to investigate the effect of the mutation in the absence of fertilization. Stamens were removed from wild-type and *Atsyn3-2*$^{+/-}$ flowers at stage 12 (Smyth *et al.*, 1990), and the pistils were subsequently analyzed by CLSM 4 and 9 days after emasculation. Four days after emasculation, pistils from wild-type plants contained a mixture of FG7 embryo sacs, in which the synergid cells, egg and central cell were undergoing senescence (Figure 6a), embryo sacs containing a degenerated cytoplasm (Figure 6b), and totally collapsed ovules (Figure 6c). Without fertilization, the integuments failed to enlarge. Female gametophytes at similar stages of degeneration, which we predicted to be wild-type gametophytes, were observed in pistils of *Atsyn3-2*$^{+/-}$ plants. However embryo sacs exhibiting other alterations were also observed. Approximately 7% of ovules (16/237) in the siliques of *Atsyn3-2*$^{+/-}$ plants contained embryo sacs in which the egg nucleus appeared to be degrading but the nuclear membrane of the central cell nucleus was still well defined (Figure 6d). A more common abnormality (13%, 26/237) comprised ovules in which the egg degenerated but the central cell nucleus was still intact (Figure 6e). Embryo sacs were also observed that contained two abnormally positioned nuclei (Figure 6f,g) as well as ovules containing three or four nuclei in various positions (Figure 6h–j). Finally, a small number of embryo sacs containing up to eight nuclei were also observed (Figure 6k), suggesting that the central cell nucleus in some ovules containing the *Atsyn3-2* mutation underwent nuclear division without fertilization.

Table 1 Abnormal female gametophyte and seed development in *Atsyn3-2*$^{+/-}$ plants

			Abnormal phenotype[a]							
Wt ovule and seed developmental stage[b]	Total ovule/seed number examined	Percent abnormal	1 N ES (Fig. 5b)	2 N ES (Fig. 5c)	3 N ES (Fig. 5d)	4 N ES (Fig. 5e-h)	Degenerated ES or seed (Fig. 5a, 5i)	Central cell (Fig. 5j)	2 EN (Fig. 5k)	4-cell embryo with cellularized endosperm (Fig. 5l)
FG0-FG5	409	2.2%			2	3	4			
FG6	122	23.8%	3	5	7	11	3			
Zygote	346	22.3%	3		4	5	38	14	13	
Embryo proper	160	28.8%			3	2	29	8	4	
Four-cell embryo	171	33.9%			2	1	35	14	6	
Globular embryo	255	39.6%			3	1	78	13	2	4
Heart embryo	61	57.4%					35			

FG, female gametophyte; N, nucleus/nuclei; ES, embryo sac; EN, endosperm nuclei.
[a]Number of abnormal ovules/seeds observed in siliques of several independent inflorescences of *Atsyn3-2*$^{+/-}$ plants. Only those embryo sacs containing abnormally positioned or sized nuclei were counted as defective.
[b]Female gametophyte stages were defined according to Christensen *et al.* (1997). Ovule and seed stages were presented based on the most abundant stage in a given silique.

Nine days after emasculation, carpels from wild-type plants contained 100% shriveled/collapsed ovules (Figure 6c). In contrast, 56 of the 227 ovules (25%) observed in *Atsyn3-2*$^{+/-}$ plants were found to contain large shriveled embryo sacs (Figure 6l). The remaining 75% of the seeds were small and collapsed, resembling those observed in wild-type plants in the absence of fertilization (Figure 6c). Ovules resembling those shown in Figure 6(d–l) were never observed in the carpels of wild-type plants. Therefore, in the absence of *AtSYN3*, some embryo sacs exhibit delayed senescence and the central cell nucleus appeared to undergo a limited number of nuclear divisions prior to its arrest and degeneration. It is also possible that the multiple nuclei could result from delayed embryo sac development in mutant ovules; however, based on the position of the nuclei and the appearance of these embryo sacs, we do not believe that this is a likely possibility.

Complementation experiments were performed to determine whether the gametophyte-defective phenotype observed in *Atsyn3-2*$^{+/-}$ plants is due to the disruption of *AtSYN3*. A complementation plasmid containing an *AtSYN3* genomic fragment was introduced into *Atsyn3-2*$^{+/-}$ plants. Transformed plants were screened by BASTA selection and analyzed by PCR to monitor for the presence of the complementation construct, the *Atsyn3-2* T-DNA insert, and the wild-type *AtSYN3* genomic locus. Heterozygous plants containing the *AtSYN3* complementation clone were found to exhibit increased seed set. Specifically, in the presence of the construct, the percentage of aborted seed in *Atsyn3-2*$^{+/-}$ plants decreased from approximately 50% to wild-type levels. Furthermore, the *AtSYN3* complementation clone could rescue plants homozygous for the T-DNA insert, confirming that *AtSYN3* is essential for gametophyte development.

Discussion

Comparison of AtSYN3 with SCC1/REC8 proteins from yeast, worms, flies, other animals and plants indicates that it belongs to the α-kleisin family of proteins (Schleiffer *et al.*, 2003). Similarities in gene structure between *AtSYN2* and *AtSYN3*, including the sequence of several introns, suggested that the two genes are derived from a relatively recent duplication event (Dong *et al.*, 2001). It has recently been shown that AtSYN2/AtRAD21.1 and AtSYN4/AtRAD21.3 have redundant and overlapping functions in mitosis (da Costa-Nunes *et al.*, 2006). In contrast, our current results demonstrate that the nuclear distribution of AtSYN3 is very different from that of AtSYN2/AtRAD21.1, AtSYN4/AtRAD21.3 and other cohesin proteins in general. Furthermore, we have shown that, in contrast to other cohesin proteins, a knockout mutation in *AtSYN3* affects both male and female gametophytes. These results suggest that AtSYN3 may have evolved a unique role in

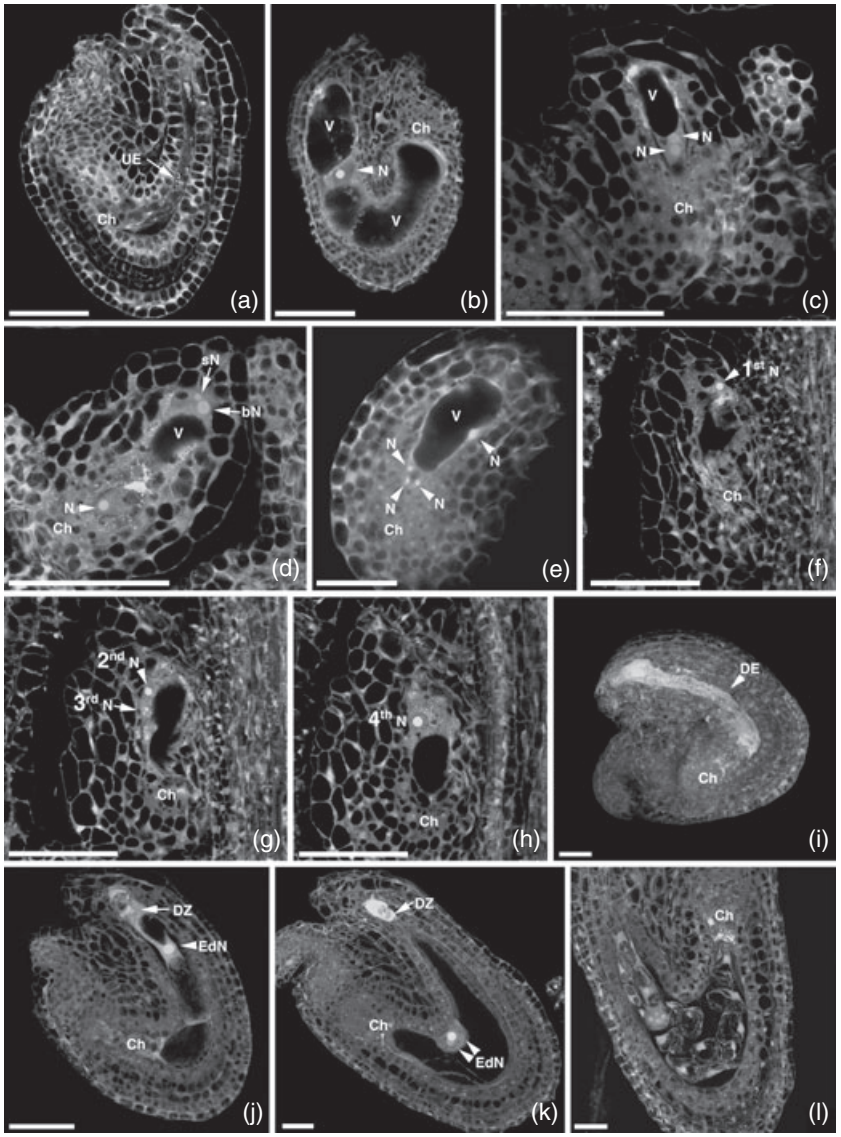

Figure 5. Female gametophyte and seed development in *Atsyn3-2*$^{+/-}$ plants.
The chalazal pole (Ch) is indicated in each micrograph. Unless otherwise noted, the images represent a single 1.5 μm optical section.
(a–h) *Atsyn3*$^{-}$ ovules in siliques that contain wild-type ovules at stage FG6; (f–h) serial optical sections of an ovule with four nuclei in the female gametophyte.
(i–l) *Atsyn3*$^{-}$ ovules after fertilization.
(a) Ovule with a degenerated and undeveloped embryo sac (UE, arrow).
(b) Ovule with one nucleus (N, arrowhead) surrounded by vacuoles (V).
(c) Ovule with two nuclei (N, arrowhead) crowded at the chalazal pole.
(d) Ovule with three nuclei. One nucleus (N, arrowhead) is at the chalazal pole, while abnormally small (sN, arrow) and large (bN, arrow) nuclei are at the other end. A projection of three 1.5 μm optical sections is shown.
(e) Ovule with four nuclei (N). A projection of two 1.5 μm optical sections is shown.
(f) Optical section of an ovule with four nuclei. The first nucleus (1st N, arrowhead) is at the micropylar pole.
(g) Optical section with the second (2nd N, arrowhead) and third nuclei (3rd N, arrow). The 3rd nucleus contains four nucleoli.
(h) Optical section with the fourth nucleus (4th N, arrowhead) at the micropylar pole.
(i) Ovule with a degenerated embryo sac (DE). A projection of five 2 μm optical sections is shown.
(j) Ovule containing one endosperm nucleus (EdN) and a degenerated zygote (DZ). A projection of two 2 μm optical sections is shown.
(k) Ovule containing two endosperm nuclei (EdN) and a degenerated zygote (DZ). A projection of three 3 μm optical sections is shown.
(l) Ovule with a quadrant embryo in which the endosperm has been cellularized. A projection of five 3 μm optical sections is shown.
Scale bar = 10 μm.

plants and may not function as part of a typical cohesin complex.

AtSYN3 localization patterns differ from those of typical α-kleisin proteins

Localization studies using anti-SYN3 antibody on wild-type Arabidopsis plants and culture cells and on transgenic plants expressing either a Myc- or YFP-tagged SYN3 transgene showed that SYN3 is a nuclear protein that is present primarily in the nucleolus from interphase to late prophase in both somatic cells and meiocytes (Figure 1). In somatic cells, strong SYN3 labeling was observed in the nucleolus from G_1 through early mitotic prophase. SYN3 signal was typically undetectable during metaphase and anaphase after nucleolar breakdown, and was observed again in late telophase as the nucleoli began to reform (data not shown). Although SYN3 was also detected in the nucleoplasm, the strongest signal was consistently observed in the nucleolus. Similar distribution patterns were observed in male meiocytes, where strong SYN3 signal was found inside the nucleolus from meiotic interphase to late diplotene when the nucleolus began to break down.

Localization studies on mitotic α-kleisins in several organisms have shown that the proteins are typically distributed over the bulk of the chromosomes from interphase to anaphase. In yeast, cohesin complexes associate with chromosomes after mitosis, with the establishment of cohesion at S phase (Michaelis *et al.*, 1997; Uhlmann and Nasmyth, 1998; Toth *et al.*, 1999). ChIP studies have shown that cohesin complexes are enriched at centromeric regions (Blat and Kleckner, 1999; Megee *et al.*, 1999; Tanaka *et al.*, 1999), as well as at narrowly defined loci every 5–10 kb along the chromosome arms, which typically represent sites of

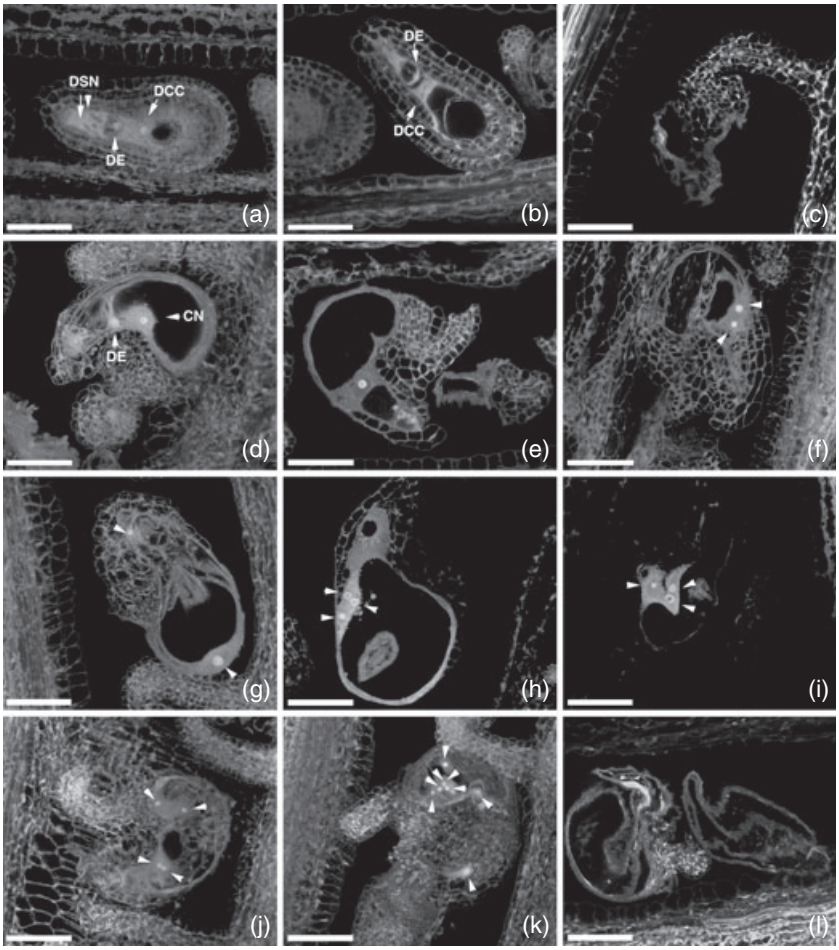

Figure 6. Ovules in wild-type and *Atsyn3-2*$^{+/-}$ plants in the absence of fertilization.
(a–c) Ovule development in wild-type flowers after emasculation.
(d–l) Abnormal *Atsyn3*$^{-}$ ovule development after emasculation.
(a) FG7 stage embryo sac containing degenerated synergids (DSN), egg (DE) and central cell (DCC) 4 days after emasculation. A projection of three 1.5 μm optical sections is shown.
(b) Embryo sac at a later stage of degeneration than (a). The cytoplasm of the degenerated egg (DE) and central cell (DCC) obscures the nuclei 4 days after emasculation. A projection of two 1.5 μm optical sections is shown.
(c) Shriveled ovule 4 and 9 days after emasculation. The embryo sac and the integuments have degenerated. A single 1.5 μm optical section is shown.
(d) Embryo sac with a degenerated egg (DE) and a central cell (nucleus, CN). No sign of degeneration in the central cell nucleus is observed. A projection of three 2 μm optical sections is shown.
(e) Embryo sac with a single nucleus. Note the well-defined nuclear membrane. A single 2 μm optical section is shown.
(f) Embryo sac with two nuclei (arrowheads). A projection of two 2 μm optical sections is shown.
(g) Ovule with two nuclei (arrowheads) of different sizes at opposite poles of the embryo sac. Note that the nuclear membrane of the larger nucleus is intact and well defined. A projection of three 3 μm optical section is shown.
(h) Ovule with three overlapping nuclei (arrowheads). A single 3 μm optical section is shown.
(i) Ovule with three nuclei (arrowheads) of different shapes. The cytoplasm is very bright and the ovule is shriveled. A single 3 μm optical section is shown.
(j) Ovule with four nuclei (arrowheads). Two nuclei are grouped at one pole with the other two at the opposite pole. A projection of three 3 μm optical sections is shown.
(k) Ovule with eight nuclei (arrowheads). One nucleus is at one pole of the embryo sac, two nuclei are in the center, and the remaining five are grouped together. A projection of six 3 μm optical sections is shown.
(l) Two large shriveled ovules that lack any nucellar or integument tissue. A projection of two 3 μm optical sections.
Scale bar = 50 μm.

convergent transcription (Glynn *et al.*, 2004; Lengronne *et al.*, 2004). In animal cells, cohesin–chromatin interactions begin at telophase when cohesin subunits are found loosely associated with the bulk of the chromatin. After DNA replication, the interactions become more stable (Gerlich *et al.*, 2006). A portion of the cohesin complexes disassociates from chromosomes during mitotic prophase in a process that requires the polo and aurora kinases, while a population remains bound to the chromosomes until it is cleaved by separase at the onset of anaphase (Losada

et al., 1998; Darwiche *et al.*, 1999; Sumara *et al.*, 2000; Waizenegger *et al.*, 2000; Warren *et al.*, 2000; Losada *et al.*, 2002; Sumara *et al.*, 2002). Although the Arabidopsis condensin protein AtCAP-H2 has been found to localize preferentially in the nucleolus of somatic cells (Fujimoto *et al.*, 2005), α-kleisins have not previously been found to be enriched in the nucleolus. Therefore, the distribution of AtSYN3 is quite different from that of other α-kleisin proteins.

Unlike other mutations in plant cohesin proteins, the Atsyn3-2 mutation causes gametophytic lethality

Heterozygous *Atsyn3-2*$^{+/-}$ plants exhibit non-Mendelian inheritance patterns, segregating as 3:1:0 (wild-type: heterozygote:homozygote). We found that the mutation causes 100% female gametophytic lethality and is passed through the pollen at a significantly reduced level. Pollen in *Atsyn3-2*$^{+/-}$ plants appears to develop normally. However, subtle alterations in shape are observed in approximately 30% of the pollen from *Atsyn3-2*$^{+/-}$ plants, and a relatively large percentage of pollen grains from *Atsyn3-2*$^{+/-}$ plants are unable to germinate under *in vitro* assay conditions. Furthermore, the presence of > 50% aborted seeds in the siliques of *Atsyn3-2*$^{+/-}$ plants raises the possibility that some *Atsyn3-2*$^{-}$ pollen germinates but is defective in fertilization. This is consistent with our observation that the mutation is passed through pollen at rates approximately one quarter of the level expected if the mutation did not affect the male gametophyte (3:1 versus 1:1 wild-type:heterozygote). Experiments are currently underway to identify the specific nature of the pollen defect and determine how it affects pollen germination/function.

Although the *Atsyn3-2*$^{+/-}$ mutation causes complete female gametophyte lethality, the effect of the mutation is somewhat variable. Our analysis of megagametogenesis in *Atsyn3-2*$^{+/-}$ plants showed that approximately 50% of *Atsyn3-2*$^{-}$ embryo sacs appear to arrest by approximately FG6, and show signs of degradation by FG8 (Table 1). Embryo sacs with one, two, three or four nuclei were identified in pistils containing wild-type FG6 embryo sacs, suggesting that the mutation may affect mitosis and that the effect of the mutation is cumulative through successive mitotic divisions. However, the presence of irregularly spaced nuclei in most *Atsyn3-2*$^{-}$ embryo sacs raises the possibility that the mutation may also affect nuclear migration or some other aspect of megagametogenesis. Approximately half of the *Atsyn3-2*$^{-}$ ovules appeared to develop through FG8, and were fertilized, but arrested at the zygote stage. The *Atsyn3-2* T-DNA insert is in exon 6 and is predicted to result in a complete knockout of the gene. However, we cannot rule out the possibility that a truncated version of the protein is produced and partially functional, resulting in the phenotypic variability that we observe. It is also possible that the phenotypic variability is the result of unequal partitioning of the wild-type protein during meiosis. As described below, phenotypic variability has been observed for several other female gametophytic mutants.

Mutations in several proteins essential for the formation or release of cohesion have been characterized in plants, including SMC1, SMC3, SCC3 and ESP1 (Liu *et al.*, 2002; Chelysheva *et al.*, 2005; Liu and Makaroff, 2006). In each case, the mutations resulted in embryo lethality, but appeared to be passed normally through the gametes. Knockout mutations in *SMC1* and *SMC3*, which are core components of the cohesin complex, exhibit strong titan phenotypes, with significant defects in early embryo development and enlarged endosperm nuclei and nucleoli (Liu *et al.*, 2002). A knockout mutation in *SCC3*, another component of the core cohesin complex, has also been shown to cause embryo lethality, although the specific nature of the defect has not been determined (Chelysheva *et al.*, 2005). Finally, mutations in *AESP1*, which facilitates the release of cohesion at the metaphase to anaphase transition, blocks embryo development at approximately the globular stage of development and causes a weak titan phenotype (Liu and Makaroff, 2006). While the Arabidopsis cohesin genes are clearly essential for embryo development, none of the previous mutations appeared to affect gametophyte development, as all are passed apparently normally through the gametes. Therefore, SYN3 is the only plant cohesin-associated protein that has been shown to be essential for gametophyte development.

Given that cohesions are essential for nuclear division, the observation that mutations in many of the cohesin proteins do not cause gametophyte lethality is quite surprising. It has been suggested that the ability of gametes to develop normally in the presence of null mutations in genes essential for cellular division may reflect the diffusion of trace amounts of functional protein from surrounding heterozygous tissues into the gametes (Liu *et al.*, 2002). It is also possible that meiotic cells contain a pool of protein or mRNA that allows several rounds of nuclear division to occur before the effect of the mutation can be observed (Liu and Makaroff, 2006). If true, then this suggests that either *AtSYN3* mRNA and/or protein is turned over relatively quickly, or that the absolute level of SYN3 is more critical than for the other cohesin proteins.

What is the role of AtSYN3?

A relatively large number of female gametophytic mutations have been identified in Arabidopsis. Phenotypes observed range from embryo sacs that arrest with one functional megaspore to those that are fertilized but arrest during early embryo development. While many of the mutations appear to block embryo sac development at a specific stage, several

mutations result in the production of embryo sacs with variable numbers and positions of nuclei (Pagnussat *et al.*, 2005), similar to our observations for *Atsyn3-2*. For example, the *hadad* (*hdd*) mutation results in female gametophyte arrest over a wide range of developmental stages, with embryo sacs arresting at the two-, four- or eight-nucleate stages (Moore *et al.*, 1997). Likewise, mutations in a number of genes, including a guanine nucleotide exchange factor (At1g01960), a *dc1* domain protein (At1g55420), a mitochondrial RNA helicase (At4g14790), and two proteins involved in rRNA processing (At2g47990 and At3g60360), result in variable numbers and positions of embryo sac nuclei (Pagnussat *et al.*, 2005). The best characterized of these mutations is in the *slowwalker1* (*SWA1*, At2g47990) gene (Shi *et al.*, 2005). *SWA1* encodes a WD40 repeat-containing protein that is required for the proper processing of 18S rRNA precursors. The *swa1* mutation causes asynchronous megagametophyte development, resulting in embryo sacs that arrest at the two-, four- and eight-nucleate stages. Similar to our observations for *Atsyn3-2*, the *swa1* mutation also shows reduced penetrance through the male gametophyte, and the SWA1 protein localizes in the nucleolus. However, in contrast to our observations for the *Atsyn3-2* mutation, *swa1* female gametophytes could be fertilized by delayed manual fertilization. Also, although we observed what appeared to be a fertilization-independent nuclear division of the central cell nucleus in some *Atsyn3-2* embryo sacs, this was not reported for the *swa1* mutation. Similarities between *Atsyn3-2* and *swa1* raise the possibility that SYN3 may be required for proper rDNA transcription and/or processing.

ChIP experiments in yeast have shown that a portion of the yeast SCC1 population binds to rDNA repeats, where it suppresses unequal recombination between sister chromatids (Kobayashi *et al.*, 2004). Activation of transcription from E-pro within the rDNA spacer displaces SCC1, and results in increased recombination at the rDNA loci and gene amplification (Kobayashi and Ganley, 2005). SYN3 could also have evolved to specifically fulfil this role of maintaining cohesion at the rDNA loci in plant cells. In yeast, SCC1 appears to function as part of a normal cohesin complex at the rDNA loci. Immunolocalization studies using antibodies against the Arabidopsis cohesin proteins SMC3 and SCC3 failed to detect significant labeling in the nucleolus (Chelysheva *et al.*, 2005; Lam *et al.*, 2005), suggesting that SYN3 may function independently of the other core cohesin components. However, it is also possible that structural/conformational considerations prevented the SMC3 and SCC3 antibodies from detecting the proteins in the nucleolus.

Unlike the cohesins, several condensins have been found in the nucleolus of somatic cells and play important roles in rDNA structure and expression (Uzbekov *et al.*, 2003; Machin *et al.*, 2004; Fujimoto *et al.*, 2005). In budding yeast, the condensin subunits YCS4 and SMC4 are uniformly distributed throughout the nucleus from G_1 to metaphase. As cells enter anaphase, the proteins become highly enriched in the nucleolus (Freeman *et al.*, 2000). Localization of condensin to the nucleolus is required to correctly partition the rDNA, which is ultimately required for its segregation (D'Amours *et al.*, 2004; Sullivan *et al.*, 2004; Yu and Koshland, 2005). Yeast condensin has also been implicated in arranging rDNA repeats into heterochromatic-like structures that are important for the delineation of silencing domains (Machin *et al.*, 2004). In *Xenopus* cells, condensins are found in the nucleus and in the nucleolus throughout the cell cycle (Uzbekov *et al.*, 2003). In the nucleolus, they are not tightly associated with the rDNA, which raises the possibility that they may participate in rRNA synthesis and/or processing, or have a scaffolding role in the spatial organization of the nucleolus (Uzbekov *et al.*, 2003). Finally, Arabidopsis CAP-H2, a γ-kleisin, which is part of the condensin II complex, localizes predominantly to the nucleolus throughout the cell cycle (Fujimoto *et al.*, 2005), similar to our observations for SYN3. This raises the interesting possibility that SYN3 could function as part of a condensin complex in the nucleolus, and may be involved in controlling rDNA structure or expression. However, similarities between the *Atsyn3-2* and *swa1* mutations also raise the possibility that SYN3 could be involved in rRNA synthesis and/or processing.

In summary, we have shown that SYN3 has non-overlapping functions with the three other Arabidopsis α-kleisin proteins. It localizes predominantly to the nucleolus of both somatic and meiotic cells and is required for both male and female gametophyte development. These results suggest that SYN3 may not function as part of a typical cohesin complex, but rather may have evolved a specialized role in the nucleolus, possibly as part of a condensin-like complex that functions to control rDNA structure and/or expression. Further experiments are underway to investigate this intriguing possibility.

Experimental procedures

Plant material and growth conditions

Plants were grown in Metro-Mix 200 soil (Scotts-Sierra Horticultural Products Co.; http://www.scotts.com) in a growth chamber at 22°C with a 16 h light/8 h dark cycle. Ten days after germination, leaves were collected from rosette-stage plants. After 16–18 days, buds with lengths between 0.5 and 0.7 mm were collected from pre-bolting plants for the analysis of meiosis. Roots were collected from seeds grown on agar plates. *Arabidopsis thaliana* (L.) Heynh, ecotype Wassilewskija (WS), was used in plant transformation studies using the floral dip method (Clough and Bent, 1998). Crossing studies were conducted with Columbia (Col) and WS ecotypes.

Arabidopsis suspension culture cells (Landsberg *erecta*, L*er*), kindly provided by Jonathan Jones (Sainsbury Laboratory,

Norwich, UK), were cultured in Gamborg's suspension cell medium (4.5 g l^{-1} Murashige and Skoog basal salts, 3% w/v sucrose, 0.59 g l^{-1} MES, 0.5 mg l^{-1} of 1-naphthaleneacetic acid (NAA), 0.05 mg l^{-1} benzylaminopurine (6-BA), pH 5.7) at 110 rpm at room temperature.

Molecular analysis and complementation of AtSYN3 T-DNA knockout mutations

The SALK119629 T-DNA insertion line was obtained from the Arabidopsis Biological Resource Center, while the 09510A T-DNA insertion line was obtained from the German Plant Genomics Research Program Stock Center. Genomic DNA was isolated from plants grown from seeds for the two T-DNA insertion lines, and genotyped by PCR with a set of plant-specific primers and a set of one plant-specific primer and one left border primer. SALK119629 plants were screened with primers Syn3-11 (5′-ACTCGTCCAGATTTAGTGC-3′) and 473-Salk-LBa1 (5′-ATGGTTCACGTAGTGGGCCATC-3′) and Syn3-11 and 568 (5′-TGCGTCTATTTGCCTATGA-3′) to detect the T-DNA insertion and wild-type loci, respectively. The 09510A insertion line was genotyped by PCR using primer pairs Syn3-12 (5′-AGATGGCTGAAGCACCAGTTG-3′) and LB-8409 (5′-ATATTGACCATCATACTCATTGC-3′) for the T-DNA insert, and Syn3-12 and 774 (5′-TCTGTTACTTTGCCTCAAGCACTA-3′) for the wild-type locus. In each case, an amplification product of the expected size was obtained, cloned and sequenced to confirm the presence of the T-DNA insert, after which the SALK119629 and 09510A T-DNA insertion lines were renamed *Atsyn3-1* and *Atsyn3-2*, respectively.

Southern blot analysis was conducted on *Atsyn3-1* homozygous plants to confirm that the plants were in fact homozygous, and on *Atsyn3-2*$^{+/-}$ plants to confirm that there was only one T-DNA insert. *Atsyn3-1* genomic DNA was isolated, digested with *Hin*dIII, and hybridized with a ^{32}P-labeled probe containing *AtSYN3* sequences that span the T-DNA insert. *Atsyn3-2* genomic DNA was isolated, digested with *Eco*RI, and hybridized with a ^{32}P-labeled T-DNA probe. Radioactivity was detected with a PhosphorImager (Molecular Dynamics; http://www.mdyn.com).

The distribution of *SYN3* transcripts in wild-type and *Atsyn3-1*$^{-/-}$ plants was investigated using RT-PCR. Equal amounts (4 μg) of total RNA isolated from leaves, stems, roots and buds were used to synthesize cDNA using a Thermoscript™ RT-PCR system (Invitrogen; http://www.invitrogen.com/). RT-PCR using *ACTIN 8* (*ACT8*) primers was used to standardize the amount of cDNA from different tissues (An *et al.*, 1996).

A 6742 bp genomic DNA fragment containing *SYN3* coding and 5′ and 3′ flanking sequences was amplified and cloned into the binary vector pFGC5941 for molecular complementation. The construct was introduced into *Atsyn3-2*$^{+/-}$ plants using the floral dip transformation method (Clough and Bent, 1998). *Atsyn3-2*$^{+/-}$ and *Atsyn3-2*$^{-/-}$ plants containing SYN3-pFGC5941 were identified by PCR-based genotyping using primer pairs 774 and 934 (5′-CATGCGATCATAGGCGTCTCGC-3′) for the transgene, Syn3-12 and 774 for the wild-type genomic locus, and Syn3-12 and LB-8409 for the T-DNA insert locus, in separate PCR reactions.

Morphological analysis of Atsyn3-2 *plants*

Ovule development was analyzed in *Atsyn3-2*$^{+/-}$ plants by laser scanning confocal microscopy essentially as described by Christensen *et al.* (1997). Images were collected and projected with Olympus FluoView 2.0 software (http://www.olympus-global.com/), and analyzed using Image Pro Plus (Media Cybernetics; http://www.mediacy.com) and PHOTOSHOP version 7.0 (Adobe; http://www.adobe.com).

Pollen morphology, viability and germination were compared in newly opened flowers of *Atsyn3-2*$^{+/-}$ plants and wild-type siblings from the same pot. Pollen viability was analyzed by soaking the grains in 8 μl TTC (1.0% by weight in 50% sucrose) at 37°C for 30 min (Huang *et al.*, 2004) followed by observation with an Olympus fluorescence microscope. Mitosis during pollen development was analyzed by DAPI staining (2 mg l^{-1}) followed by observation with an Olympus fluorescence microscope. Pollen germination was tested according to the method described by Fan *et al.* (2001).

Pollen morphology was analyzed using scanning electron microscopy (SEM). Freshly opened flowers of wild-type and *Atsyn3-2*$^{+/-}$ plants were fixed in 2% w/v paraformaldehyde and 5% w/v glutaraldehyde in 0.05 M cacodylate buffer (pH 7.2) overnight, rinsed three times in the same solution, and dehydrated in a graded ethanol series (30 min in each of the 10% increments). Once in 85% ethanol, the anthers were dissected, further dehydrated up to 100% ethanol, and critical point-dried with CO_2. The fixed stamens and air-dried stamens were mounted on SEM stubs with carbon tabs, sputter-coated with 21 nm gold particles, viewed and photographed using a Zeiss Supra 35 FEG-VP scanning electron microscope (http://www.zeiss.com/).

For light microscopy, isolated buds were fixed in 2.5% w/v paraformaldehyde and 4% w/v glutaraldehyde in 0.5 mol l^{-1} sodium phosphate buffer (pH 7.2) at room temperature for 2 h, then transferred to fresh fixative and kept at 4°C for 24 h. The fixed samples were rinsed with the same fixation buffer and post-fixed in 1% w/v osmium tetroxide (OsO_4) overnight at room temperature in the same fixation buffer. After a second rinse with fixation buffer, the samples were treated overnight at room temperature with 2% uranyl acetate in double-distilled water. The samples were then rinsed in double-distilled water, dehydrated in an ascending acetone series, and the anthers infiltrated and embedded in Spurr's resin (Spurr, 1969). Microtome sections (0.5 μm) were cut, placed on glass slides, and stained with cresyl violet acetate (1% in double-distilled water). Sections were examined and photographed using an Olympus AX-70 microscope (http://www.olympus-global.com) with a Photometrics digital camera (http://www.photomet.com).

SYN3 localization studies

An 813 bp fragment of the *AtSYN3* cDNA (nucleotides 715–1530, encoding amino acids 239–510), was cloned into pET-24b, expressed as a His-tagged protein in *Escherichia coli* BL21 RIL cells, and purified by Ni affinity chromatography (Clontech; http://www.clontech.com/). The over-expressed protein was analyzed by Sodium dodecyl sulphate–Polyacrylamide-gel electrophoresis and MALDI-TOF mass spectroscopy to confirm its identity. Purified protein was used to raise polyclonal antibodies in rabbits using standard procedures (Harlow and Lane, 1988). Pre-immune and anti-SYN3 sera were tested using Western blots containing the recombinant protein and total protein from wild-type plants and Arabidopsis culture cells.

The anti-SYN3 antibody was used in immunolocalization studies on Arabidopsis suspension cells and somatic and meiotic cells from wild-type anthers essentially as described previously (Cai *et al.*, 2003). Samples were observed and images captured using an Olympus 1X81 fluorescence deconvolution microscope system. Data were analyzed as described above.

Transgenic plants expressing SYN3–YFP and SYN3-Myc-tagged proteins were generated and used to analyze SYN3 distribution patterns. A 6742 bp genomic DNA fragment containing the *AtSYN3*

coding region and 2482 bp of 5′ flanking sequence was amplified by PCR and cloned in-frame with YFP in pFGC5941 to produce pFGC5941-SYN3-genomic-YFP. A Myc-tagged version (pFGC5941-SYN3-genomic-Myc) of SYN3 was constructed by replacing the YFP with Myc (Evan *et al.*, 1985). The constructs were introduced into wild-type Arabidopsis WS plants. Transgenic plants were identified by BASTA selection and the presence of the transgene confirmed by PCR.

The distribution of SYN3-Myc was monitored by immunolocalization on anther squashes from pFGC5941-SYN3-genomic-Myc transgenic plants using mouse anti-Myc antibody and Alexa-488-labeled goat antimouse antibody as described above. The distribution of SYN3–YFP during mitosis and meiosis in anther squashes of pFGC-SYN3-genomic-YFP transgenic plants was monitored directly with a YFP filter set (http://www.olympus-global.com).

Acknowledgments

We are grateful to Richard Edelman and Matthew L. Duley for technical support on the microscope, Rich Jorgenson (University of Arizona) for providing the pFGC5941 plasmid and Jonathan Jones for the Arabidopsis culture cells. We would like to thank Meghan Holdorf and Kingsley Boateng for helpful discussions and comments on the manuscript. The SALK T-DNA insertion line 119/629 was obtained from the Arabidopsis Biological Resource Center. This research was supported by grant MCB0322171 to C.A. Makaroff from the NSF.

References

An, Y., McDowell, J., Huang, S., McKinney, E., Chambliss, S. and Meagher, R. (1996) Strong, constitutive expression of the Arabidopsis ACT2/ACT8 actin subclass in vegetative tissues. *Plant J.* **10**, 107–121.

Bai, X., Peirsion, B., Dong, F., Cai, X. and Makaroff, C. (1999) Isolation and characterization of SYN1, a RAD21-like gene essential for meiosis in Arabidopsis. *Plant Cell*, **11**, 417–430.

Bhatt, A.M., Lister, C., Page, T., Fransz, P., Findlay, K., Jones, G.H., Dickinson, H.G. and Dean, C. (1999) The DIF1 gene of Arabidopsis is required for meiotic chromosome segregation and belongs to the REC8/RAD21 cohesin gene family. *Plant J.* **19**, 463–472.

Birkenbihl, R.P. and Subramani, S. (1992) Cloning and characterization of *rad21*, an essential gene of *Schizosaccharomyces pombe* involved in double-strand-break repair. *Nucleic Acids Res.* **20**, 6605–6611.

Blat, Y. and Kleckner, N. (1999) Cohesins bind to preferential sites along yeast chromosome III, with differential regulation along arms versus the centric region. *Cell*, **98**, 249–259.

Cai, X., Dong, F.G., Edelmann, R.E. and Makaroff, C.A. (2003) The Arabidopsis SYN1 cohesin protein is required for sister chromatid arm cohesion and homologous chromosome pairing. *J. Cell Sci.* **116**, 2999–3007.

Chelysheva, L., Diallo, S., Vezon, D. *et al.* (2005) AtREC8 and AtSCC3 are essential to the monopolar orientation of the kinetochores during meiosis. *J. Cell Sci.* **118**, 4621–4632.

Christensen, C.A., King, E.J., Jordan, J.R. and Drews, G.N. (1997) Megagametogenesis in *Arabidopsis* wild type and the Gf mutant. *Sex. Plant Reprod.* **10**, 49–64.

Christensen, C.A., Subramanian, S. and Drews, G.N. (1998) Identification of gametophytic mutations affecting female gametophyte development in Arabidopsis. *Dev. Biol.* **202**, 136–151.

Clough, S.J. and Bent, A.F. (1998) Floral dip: a simplified method for *Agrobacterium*-mediated transformation of *Arabidopsis thaliana*. *Plant J.* **16**, 735–743.

da Costa-Nunes, J.A., Bhatt, A.M., O'Shea, S., West, C.E., Bray, C.M., Grossniklaus, U. and Dickinson, H.G. (2006) Characterization of the three *Arabidopsis thaliana* RAD21 cohesins reveals differential responses to ionizing radiation. *J. Exp. Bot.* **57**, 971–983.

D'Amours, D., Stegmeier, F. and Amon, A. (2004) Cdc14 and condensin control the dissolution of cohesin- independent chromosome linkages at repeated DNA. *Cell*, **117**, 455–469.

Darwiche, N., Freeman, L.A. and Strunnikov, A. (1999) Characterization of the components of the putative mammalian sister chromatid cohesion complex. *Gene*, **233**, 39–47.

Dong, F., Cai, X. and Makaroff, C. (2001) Cloning and characterization of two Arabidopsis genes that belong to the RAD21/REC8 family of chromosome cohesin proteins. *Gene*, **271**, 99–108.

Evan, G.I., Lewis, G.K., Ramsay, G. and Bishop, J.M. (1985) Isolation of monoclonal antibodies specific for human c-*myc* proto-oncogene product. *Mol. Cell. Biol.* **5**, 3610–3616.

Fan, L., Wang, Y., Wang, H. and Wu, W. (2001) In vitro Arabidopsis pollen germination and characterization of the inward potassium currents in Arabidopsis pollen grain protoplasts. *J. Exp. Bot.* **52**, 1603–1614.

Freeman, L., AragonAlcaide, L. and Strunnikov, A. (2000) The condensin complex governs chromosome condensation and mitotic transmission of rDNA. *J. Cell Biol.* **149**, 811–824.

Fujimoto, S., Yonemura, M., Matsunaga, S., Nakagawa, T., Uchiyama, S. and Fukui, K. (2005) Characterization and dynamic analysis of Arabidopsis condensin subunits, AtCAP-H and AtCAP-H2. *Planta*, **222**, 293–300.

Gerlich, D., Koch, B., Dupeux, F., Peters, J.M. and Ellenberg, J. (2006) Live-cell imaging reveals a stable cohesin–chromatin interaction after but not before DNA replication. *Curr. Biol.* **16**, 1571–1578.

Glynn, E.F., Megee, P.C., Yu, H.G., Mistrot, C., Unal, E., Koshland, D.E., DeRisi, J.L. and Gerton, J.L. (2004) Genome-wide mapping of the cohesin complex in the yeast *Saccharomyces cerevisiae*. *PLoS Biol.* **2**, 1325–1339.

Golubovskaya, I.N., Hamant, O., Timofejeva, L., Wang, C.J.R., Braun, D., Meeley, R. and Cande, W.Z. (2006) Alleles of *afd1* dissect REC8 functions during meiotic prophase I. *J. Cell Sci.* **119**, 3306–3315.

Haering, C.H., Lowe, J., Hochwagen, A. and Nasmyth, K. (2002) Molecular architecture of SMC proteins and the yeast cohesin complex. *Mol. Cell*, **9**, 773–788.

Haering, C.H., Schoffnegger, D., Nishino, T., Helmhart, W., Nasmyth, K. and Lowe, J. (2004) Structure and stability of cohesin's Smc1–kleisin interaction. *Mol. Cell*, **15**, 951–964.

Harlow, E. and Lane, D. (1988) *Antibodies: A Laboratory Manual*. Cold Spring Harbor, NY: Cold Spring Harbor Laboratory Press.

Hauf, S., Roitinger, E., Koch, B., Dittrich, C.M., Mechtler, K. and Peters, J.M. (2005) Dissociation of cohesin from chromosome arms and loss of arm cohesion during early mitosis depends on phosphorylation of SA2. *PLoS Biol.* **3**, 419–432.

Huang, Z., Zhu, J., Mu, X. and Lin, J. (2004) Pollen dispersion, pollen viability and pistil receptivity in *Lenmus chinensis*. *Ann. Bot.* **93**, 295–301.

Kim, S., Xu, B. and Kastan, M. (2002) Involvement of the cohesin protein, Smc1, in Atm-dependent and independent responses to DNA damage. *Genes Dev.* **16**, 560–570.

Klein, F., Mahr, P., Galova, M., Buonomo, S.B.C., Michaelis, C., Nairz, K. and Nasmyth, K. (1999) A central role for cohesions in sister chromatid cohesion, formation of axial elements and recombination during yeast meiosis. *Cell*, **98**, 91–103.

Kobayashi, T. and Ganley, A.R.D. (2005) Recombination regulation by transcription-induced cohesin dissociation in rDNA repeats. *Science*, **309**, 1581–1584.

Kobayashi, T., Horiuchi, T., Tongaonkar, P., Vu, L. and Nomura, M. (2004) SIR2 regulates recombination between different rDNA repeats, but not recombination within individual rRNA genes in yeast. *Cell*, **117**, 441–453.

Lam, W.S., Yang, X.H. and Makaroff, C.A. (2005) Characterization of *Arabidopsis thaliana* SMC1 and SMC3: evidence that ASMC3 may function beyond chromosome cohesion. *J. Cell Sci.* **118**, 3037–3048.

Lengronne, A., Katou, Y., Mori, S., Yokobayashi, S., Kelly, G.P., Itoh, T., Watanabe, Y., Shirahige, K. and Uhlmann, F. (2004) Cohesin relocation from sites of chromosomal loading to places of convergent transcription. *Nature*, **430**, 573–578.

Liu, Z. and Makaroff, C.A. (2006) Arabidopsis separase AESP is essential for embryo development and the release of cohesin during meiosis. *Plant Cell*, **18**, 1213–1225.

Liu, C., McElver, J., Tzafrir, I., Joosen, R., Wittich, P., Patton, D., Van Lammeren, A. and Meinke, D. (2002) Condensin and cohesin knockouts in Arabidopsis exhibit a titan seed phenotype. *Plant J.* **29**, 405–415.

Losada, A. and Hirano, T. (2005) Dynamic molecular linkers of the genome: the first decade of SMC proteins. *Genes Dev.* **19**, 1269–1287.

Losada, A., Hirano, M. and Hirano, T. (1998) Identification of Xenopus SMC protein complexes required for sister chromatid cohesion. *Genes Dev.* **12**, 1986–1997.

Losada, A., Yokochi, T., Kobayashi, R. and Hirano, T. (2000) Identification and characterization of SA/Scc3p subunits in the Xenopus and human cohesin complexes. *J. Cell Biol.* **150**, 405–416.

Losada, A., Hirano, M. and Hirano, T. (2002) Cohesin release is required for sister chromatid resolution, but not for condensin-mediated compaction, at the onset of mitosis. *Genes Dev.* **23**, 3004–3016.

Machin, F., Paschos, K., Jarmuz, A., Torres-Rosell, J., Pade, C. and Aragon, L. (2004) Condensin regulates rDNA silencing by modulating nucleolar Sir2p. *Curr. Biol.* **14**, 125–130.

Megee, P.C., Mistrot, C., Guacci, V. and Koshland, D. (1999) The centromeric sister chromatid cohesion site directs Mcd1p binding to adjacent sequences. *Mol. Cell*, **4**, 445–450.

Michaelis, C., Ciosk, R. and Nasmyth, K. (1997) Cohesins: chromosomal proteins that prevent premature separation of sister chromatids. *Cell*, **91**, 35–45.

Mito, Y., Sugimoto, A. and Yamamoto, M. (2003) Distinct developmental function of two *Caenorhabditis elegans* homologs of the cohesin subunit Scc1/Rad21. *Mol. Biol. Cell*, **14**, 2399–2409.

Moore, J.M., Calzada, J.P.V., Gagliano, W. and Grossniklaus, U. (1997) Genetic characterization of hadad, a mutant disrupting female gametogenesis in *Arabidopsis thaliana*. *Cold Spring Harb. Symp. Quant. Biol.* **62**, 35–47.

Nasmyth, K. (2001) Disseminating the genome: joining, resolving, and separating sister chromatids during mitosis and meiosis. *Annu. Rev. Genet.* **35**, 673–745.

Nasmyth, K. and Haering, C.H. (2005) The structure and function of SMC and kleisin complexes. *Annu. Rev. Biochem.* **74**, 595–648.

Ono, T., Losada, A., Hirano, M., Myers, M.P., Neuwald, A.F. and Hirano, T. (2003) Differential contributions of condensin I and condensin II to mitotic chromosome architecture in vertebrate cells. *Cell*, **115**, 109–121.

Pagnussat, G.C., Yu, H.J., Ngo, Q.A., Rajani, S., Mayalagu, S., Johnson, C.S., Capron, A., Xie, L.F., Ye, D. and Sundaresan, V. (2005) Genetic and molecular identification of genes required for female gametophyte development and function in Arabidopsis. *Development*, **132**, 603–614.

Pasierbek, P., Jantsch, M., Melcher, M., Schleiffer, A., Schweizer, D. and Loidl, J. (2001) A *Caenorhabditis elegans* cohesion protein with functions in meiotic chromosome pairing and disjunction. *Genes Dev.* **15**, 1349–1360.

Peirson, B.N., Bowling, S.E. and Makaroff, C.A. (1997) A defect in synapsis causes male sterility in a T-DNA-tagged *Arabidopsis thaliana* mutant. *Plant J.* **11**, 659–669.

Sanders, P.M., Bui, A.Q., Weterings, K., McIntire, K.N., Hsu, Y.C., Lee, P.Y., Truong, M.T., Beals, T.P. and Goldberg, R.B. (1999) Anther developmental defects in *Arabidopsis thaliana* male-sterile mutants. *Sex. Plant Reprod.* **11**, 297–322.

Schleiffer, A., Kaitna, S., Maurer-Stroh, S., Glotzer, M., Nasmyth, K. and Eisenhaber, F. (2003) Kleisins: a superfamily of bacterial and eukaryotic SMC protein partners. *Mol. Cell*, **11**, 571–575.

Shi, D.Q., Liu, J., Xiang, Y.H., Ye, D., Sundaresan, V. and Yang, W.C. (2005) SLOW WALKER1, essential gene for gametogenesis in Arabidopsis, encodes a WD40 protein involved in 18S ribosomal RNA biogenesis. *Plant Cell*, **17**, 2340–2354.

Smyth, D.R., Bowman, J.L. and Meyerowitz, E.M. (1990) Early flower development in Arabidopsis. *Plant Cell*, **2**, 755–767.

Sonoda, E., Matsusaka, T., Morrison, C. *et al.* (2001) Scc1/Rad21/Mcd1 is required for sister chromatid cohesion and kinetochore function in vertebrate cells. *Dev. Cell*, **6**, 759–770.

Spurr, A.H. (1969) A low viscosity epoxy resin embedding medium for electron microscopy. *J. Ultrastruct. Res.* **26**, 31–43.

Strom, L., Lindroos, H.B., Shirahige, K. and Sjogren, C. (2004) Post-treplicative recruitment of cohesin to double-strand breaks is required for DNA repair. *Mol. Cell*, **16**, 1003–1015.

Sullivan, M., Higuchi, T., Katis, V.L. and Uhlmann, F. (2004) Cdc14 phosphatase induces rDNA condensation and resolves cohesin-independent cohesion during budding yeast anaphase. *Cell*, **117**, 471–482.

Sumara, I., Vorlaufer, E., Gieffers, C., Peters, B.H. and Peters, J.M. (2000) Characterization of vertebrate cohesin complexes and their regulation in prophase. *J. Cell Biol.* **151**, 749–761.

Sumara, I., Vorlaufer, E., Stukenberg, P., Kelm, O., Redemann, N., Nigg, E. and Peters, J. (2002) The dissociation of cohesin from chromosomes in prophase is regulated by polo-like kinase. *Mol. Cell*, **9**, 515–525.

Tanaka, T., Cosma, M.P., Wirth, K. and Nasmyth, K. (1999) Identification of cohesin association sites at centromeres and along chromosome arms. *Cell*, **98**, 847–858.

Toth, A., Ciosk, R., Uhlmann, F., Galova, M., Schleiffer, A. and Nasmyth, K. (1999) Yeast cohesin complex requires a conserved protein, Eco1p(Ctf7), to establish cohesion between sister chromatids during DNA replication. *Genes Dev.* **13**, 320–333.

Uhlmann, F. (2004) The mechanism of sister chromatid cohesion. *Exp. Cell Res.* **296**, 80–85.

Uhlmann, F. and Nasmyth, K. (1998) Cohesion between sister chromatids must be established during DNA replication. *Curr. Biol.* **8**, 1095–1101.

Uhlmann, F., Wernic, D., Poupart, M.A., Koonin, E.V. and Nasmyth, K. (2000) Cleavage of cohesin by the CD clan protease separin triggers anaphase in yeast. *Cell*, **103**, 375–386.

Unal, E., Arbel-Eden, A., Sattler, U., Shroff, R., Lichten, M., Haber, J.E. and Koshland, D. (2004) DNA damage response pathway uses histone modification to assemble a double-strand break-specific cohesin domain. *Mol. Cell*, **16**, 991–1002.

Uzbekov, R., Timirbulatova, E., Watrin, E., Cubizolles, F., Ogereau, D., Gulak, P., Legagneux, V., Polyakov, V.J., Le Guellec, K. and Kireev, I. (2003) Nucleolar association of pEg7 and XCAP-E, two

members of *Xenopus laevis* condensin complex in interphase cells. *J. Cell Sci.* **116**, 1667–1678.

Waizenegger, I.C., Hauf, S., Meinke, A. and Peters, J.M. (2000) Two distinct pathways remove mammalian cohesin from chromosome arms in prophase and from centromeres in anaphase. *Cell*, **103**, 399–410.

Warren, W.D., Steffensen, S., Lin, E. *et al.* (2000) The Drosophila RAD21 cohesin persists at the centromere region in mitosis. *Curr. Biol.* **10**, 1463–1466.

Yu, H.G. and Koshland, D. (2005) Chromosome morphogenesis: condensin-dependent cohesin removal during meiosis. *Cell*, **123**, 397–407.